Available online at www.sciencedirect.com

SciVerse ScienceDirect

Ceramics International 39 (2013) 8487–8492

CERAMICS INTERNATIONAL

www.elsevier.com/locate/ceramint

Short communication

Preparation of graphitic carbon nanofibres by in situ catalytic graphitisation of phenolic resins

Qinghua Hu[a,b], Xitang Wang[a,*], Zhoufu Wang[a,*]

[a]*The State Key Laboratory Breeding Base of Refractories and Ceramics, Wuhan University of Science and Technology, Wuhan 430081, China*

[b]*College of Chemical and Environmental Engineering, Jiujiang University, Jiujiang 332005, China*

Received 24 November 2012; received in revised form 5 February 2013; accepted 25 February 2013
Available online 5 March 2013

Absract

Graphitic carbon nanofibres were prepared using $NiC_2O_4 \cdot 2H_2O$ nanofibres as both the templates and catalyst precursors via the in situ catalytic graphitisation of phenolic resins. The influence of temperature on the phase and microstructure evolution of the $NiC_2O_4 \cdot 2H_2O$/phenolic resin composite was investigated by X-ray diffraction analysis, field-emission scanning electron microscopy, energy-dispersive X-ray spectroscopy, and transmission electron microscopy. The results showed that the graphitisation process begins at 1073 K, with the aid of nickel as graphitisation catalyst. The proportion of graphitic nanostructures in the carbonised sample increased with the increasing temperature. The highly crystalline nanostructures trapped in the matrix of the carbonised phenolic resins kept the fibrous morphology of the $NiC_2O_4 \cdot 2H_2O$ nanofibres. The homogeneous dispersion of the $NiC_2O_4 \cdot 2H_2O$ nanofibres in the phenolic resin determined the homogeneous formation of the graphitic carbon nanofibres in the matrix during in situ catalytic graphitisation. The fabrication of the graphitic carbon nanofibres was proposed to occur via a dissolution–precipitation mechanism.

Keywords: A. Precursors: organic; B. Fibres; B. Nanocomposites; D. Carbon

1. Introduction

Phenolic resins have been widely used as binders for carbon composites, including refractories containing carbon (RCs) such as the MgO–C and Al_2O_3–C refractories. These resins have the advantage of a high fixed carbon rate as well as high wettability with graphite and oxide, among others. RCs have efficient slag and thermal shock resistance because the carbon is not wetted by molten slag; likewise, RCs demonstrate high thermal conductivity [1]. However, the phenolic resin-pyrolysed carbon is an isotropic glassy carbon with high brittleness, which affects possible improvement of the thermal shock resistance of RCs. In addition, a high carbon content in RCs increases the carbon content of the steel product [2,3], which is detrimental to the production of low-carbon and ultra-low-carbon steels. To meet the demand for the production of low-carbon and ultra-low-carbon steels, refractories with low-carbon content have to be developed. However, the thermal shock resistance of the refractories decreases greatly with the decreasing carbon content, which consequently restricts their practical application. Several studies have focused on overcoming the poor thermal shock resistance of low-carbon MgO–C composites by adopting nanotechnology [2–5]. Nanotech magnesia–carbon bricks that utilise the nanographitic carbon were reported to possess excellent properties [6–8]. The addition of graphitic carbon improved the crushing and bending strengths before and after coking, as well as the oxidation and thermal shock resistance of the low-carbon MgO–C composite via the formation of a nanostructured matrix. Excellent high-temperature oxidation resistance was observed.

Carbon nanotubes or nanofibres with superior mechanical properties, as well as a high aspect ratio (diameter/length) and excellent thermal properties, could be used as

*Corresponding authors. Tel.: +86 27 68862388; fax: +86 27 68862529.
E-mail addresses: wangxitang@wust.edu.cn (X. Wang), whwangzf@126.com (Z. Wang).

0272-8842/$ - see front matter © 2013 Elsevier Ltd and Techna Group S.r.l. All rights reserved.
http://dx.doi.org/10.1016/j.ceramint.2013.02.081

reinforcements to develop superior nanocomposites [9–11]. Several investigations have shown that the addition of small amounts of carbon nanotubes or nanofibres can considerably improve the mechanical properties of these composites [12,13]. However, the mechanical properties of nanocomposites largely depend on the homogeneous dispersion of individual carbon nanotubes or nanofibres in the matrix because aggregated carbon nanotubes or nanofibres exhibit different mechanical behaviours from the individual nanotubes or nanofibres [13]. Thus, several efforts have been made to address the poor dispersability of nanotubes and nanofibres [14–16]. To date, the general routes are limited to chemical modification [14] or the use of a dispersant [15] for achieving homogeneous nanotube or nanofibre dispersion. However, both routes have their drawbacks and cannot be used for the commercial production of RCs, because of the high cost of the production and modification of the nanotubes or nanofibres.

To date, the methods to prepare graphitic carbon nanofibres mainly include chemical vapour deposition (CVD) [17] and electrospinning [18]. However, graphitic carbon nanofibres developed using these methods are costly and difficult to process for further applications. In the present study, we report the in situ formation of graphitic carbon nanofibres in the matrix of carbonised phenolic resins using $NiC_2O_4 \cdot 2H_2O$ nanofibres as the catalyst precursors and templates. Compared with the traditional external addition methods, the in situ formation of graphitic carbon nanofibres in the matrix of carbonised phenolic resins has several advantages. First, the glassy isotropic carbon of the phenolic resin-pyrolysed carbon can be transformed into graphitic carbon by catalytic graphitisation. Second, the aggregation of carbon nanofibres present in the matrix could be avoided by adopting the in situ formation of carbon nanofibres because the $NiC_2O_4 \cdot 2H_2O$ nanofibre catalyst precursors can be homogeneously dispersed in the matrix. Finally, the morphology, size, and concentration of the carbon nanofibres formed in the matrix can be fine-tuned by controlling the corresponding $NiC_2O_4 \cdot 2H_2O$ precursors.

2. Experimental

2.1. Synthesis

$NiC_2O_4 \cdot 2H_2O$ nanofibres were synthesised via a solvothermal reaction, as described in Ref. [19]. In a typical procedure, 0.02 mol of $NiCl_2 \cdot 6H_2O$ was placed into a 250 ml beaker, and 0.02 mol of $Na_2C_2O_4$, 60 ml of H_2O, and 100 ml of ethylene glycol (EG) were added. The mixture was stirred and sonicated for 10 min to form a green suspension. This suspension was transferred into a 250 ml Teflon-lined stainless steel autoclave. The autoclave was sealed and heated at 493 K for 24 h. After the heating treatment, the autoclave was naturally cooled to room temperature. The products were collected by filtration and washed thrice each with deionised water and absolute ethanol, respectively, before they were allowed to dry naturally in air. Thus, the $NiC_2O_4 \cdot 2H_2O$ nanofibres were obtained.

A 1 g sample of the as-synthesised $NiC_2O_4 \cdot 2H_2O$ nanofibres were dispersed in 50 ml of ethanol by ultrasonication to form a suspension, and then 40 g of the phenolic resin was added. The mixture was stirred for another 10 min and placed into a rotary evaporator. The ethanol was evaporated out of the mixture by vacuum distillation. The residue was collected and successively heat-treated at 348, 363, and 423 K for 24, 12, and 2 h, respectively. Finally, the $NiC_2O_4 \cdot 2H_2O$ nanofibre composite with the cross-linked phenolic resin (designated as NPF) was obtained.

NPF was pyrolysed and graphitised at the predefined target temperature in an electric tube furnace with Ar flow and a heating rate of 10 K/min.

2.2. Characterisation

The microstructure and element composition of the cross-linked NPF were analysed by field-emission scanning electron microscopy (FESEM), energy-dispersive X-ray

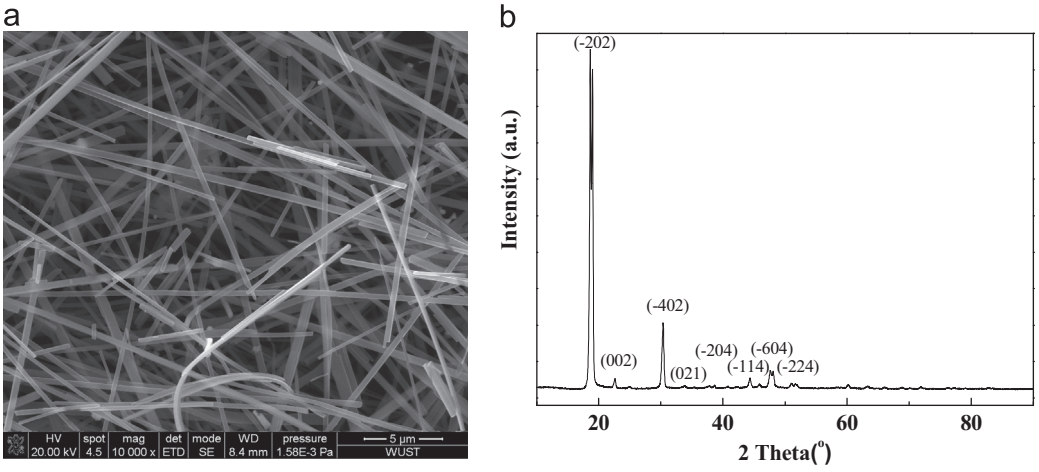

Fig. 1. SEM image (a) and XRD pattern (b) of $NiC_2O_4 \cdot SE_2O$ nanofibres.

spectroscopy (EDX), and transmission electron microscopy (TEM), combined with selected-area electron diffraction (SAED). X-ray diffraction (XRD) was used to identify the crystalline phases.

3. Results and discussion

The products obtained via the solvothermal reaction at 493 K for 24 h were characterised with XRD and SEM. The results of these analyses are shown in Fig. 1. From Fig. 1a, the obtained products are clearly composed of ultra-long nanofibres. The diameter, length, and aspect ratio of these nanofibres are approximately 100 nm, 30 μm, and 300, respectively. According to the Joint Committee on Powder Diffraction Standards (JCPDS) Card no. 25-0581, the peaks at $2\theta = 18.8^\circ$, 22.6°, 30.3°, 35.3°, 38.7°, 44.4°, 47.7°, and 51.0° (shown in Fig. 1b) can be assigned to the (−202), (002), (−402), (021), (−204), (−114), (−604), and (−224) diffraction lines of monoclinic $NiC_2O_4 \cdot 2H_2O$, respectively. This result suggested that the as-synthesised nanofibres are composed of $NiC_2O_4 \cdot 2H_2O$ with monoclinic structures [19].

The typical cross-section of the crosslinked NPF at 473 K for 2 h is shown by the SEM image in Fig. 2a, which suggests that the $NiC_2O_4 \cdot 2H_2O$ nanofibres can be tightly trapped and uniformly dispersed in the phenolic resin. The XRD pattern of the crosslinked NPF is presented in Fig. 2b. The broad diffraction peak at $2\theta = 18.5^\circ$ corresponds to the relatively orderly arrangement of adjacent polymeric chains of the phenolic resin [20,21]. All the relatively sharp diffraction peaks can be indexed to the monoclinic structure of the $NiC_2O_4 \cdot 2H_2O$ nanofibres.

To investigate the chemical transformations and structural changes of NPF that occurred during heat treatment, the samples obtained at different treatment temperatures were examined. The XRD patterns of the NPF samples treated at 773–1473 K (Fig. 3) show that the heat treatment at 773 K for 2 h provided reflexions characteristic of the Ni cubic lattice, thereby causing the characteristic reflexions of $NiC_2O_4 \cdot 2H_2O$ to disappear. Therefore, the $NiC_2O_4 \cdot 2H_2O$ trapped in the phenolic resin is completely reduced to Ni at 773 K. However, the graphitisation process has not yet begun at 773 K, as reflected by the absence of the characteristic XRD peaks of graphite. The XRD pattern corresponding to a sample prepared at 1073 K reveals the formation of graphitic carbon, which is confirmed by the appearance of the C(002) reflection at 25.9° in the XRD pattern. This reflection is superimposed on a broad band, which denotes the presence of a large fraction of amorphous carbon. The C(002) peak is rapidly sharpened, becomes more symmetric, and makes a right shift to $2\theta = 26.1^\circ$ as the temperature was increased from 1073 K to 1173 K. However, the structural characteristics of the materials, such as the average interlayer spacing (d_{002}) deduced from the XRD patterns, were hardly changed (d_{002} of 0.341–0.343 nm) as the temperature increased from 1173 K to 1473 K. Therefore, the critical graphitisation temperature seemed to be approximately 1173 K. Meanwhile, the intensity of the C(002) band increased while the broad band corresponding to

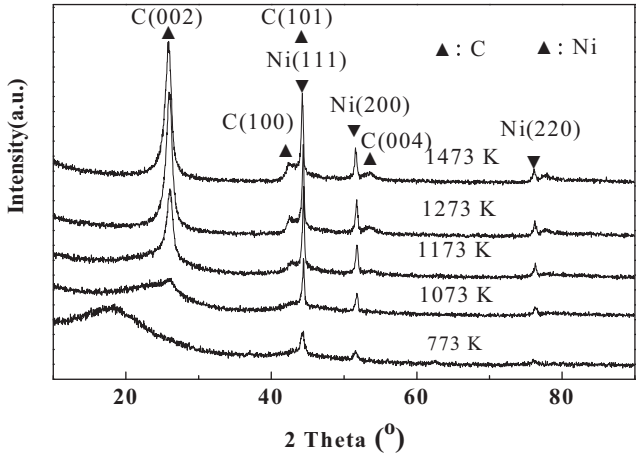

Fig. 3. XRD patterns of the $NiC_2O_4 \cdot 2H_2O$/phenolic resin composite at different temperatures.

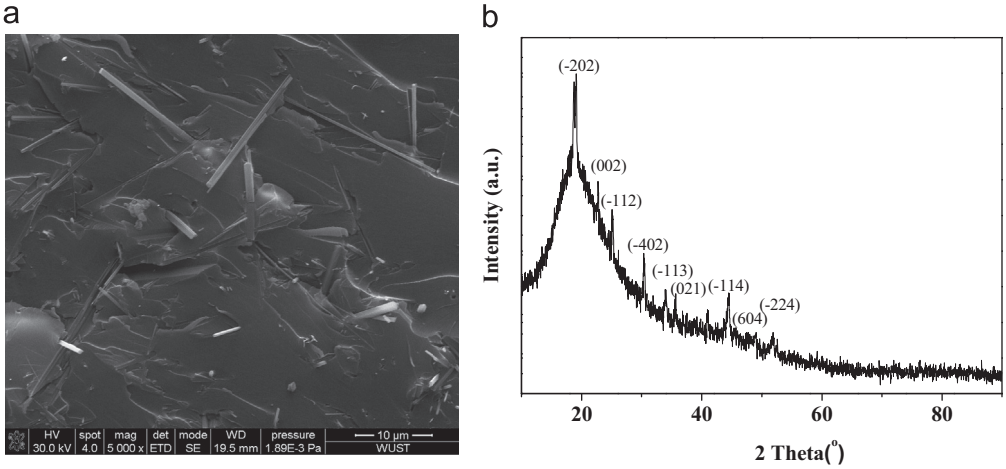

Fig. 2. SEM image (a) and XRD pattern (b) of the $NiC_2O_4 \cdot 2H_2O$/phenolic resin composite.

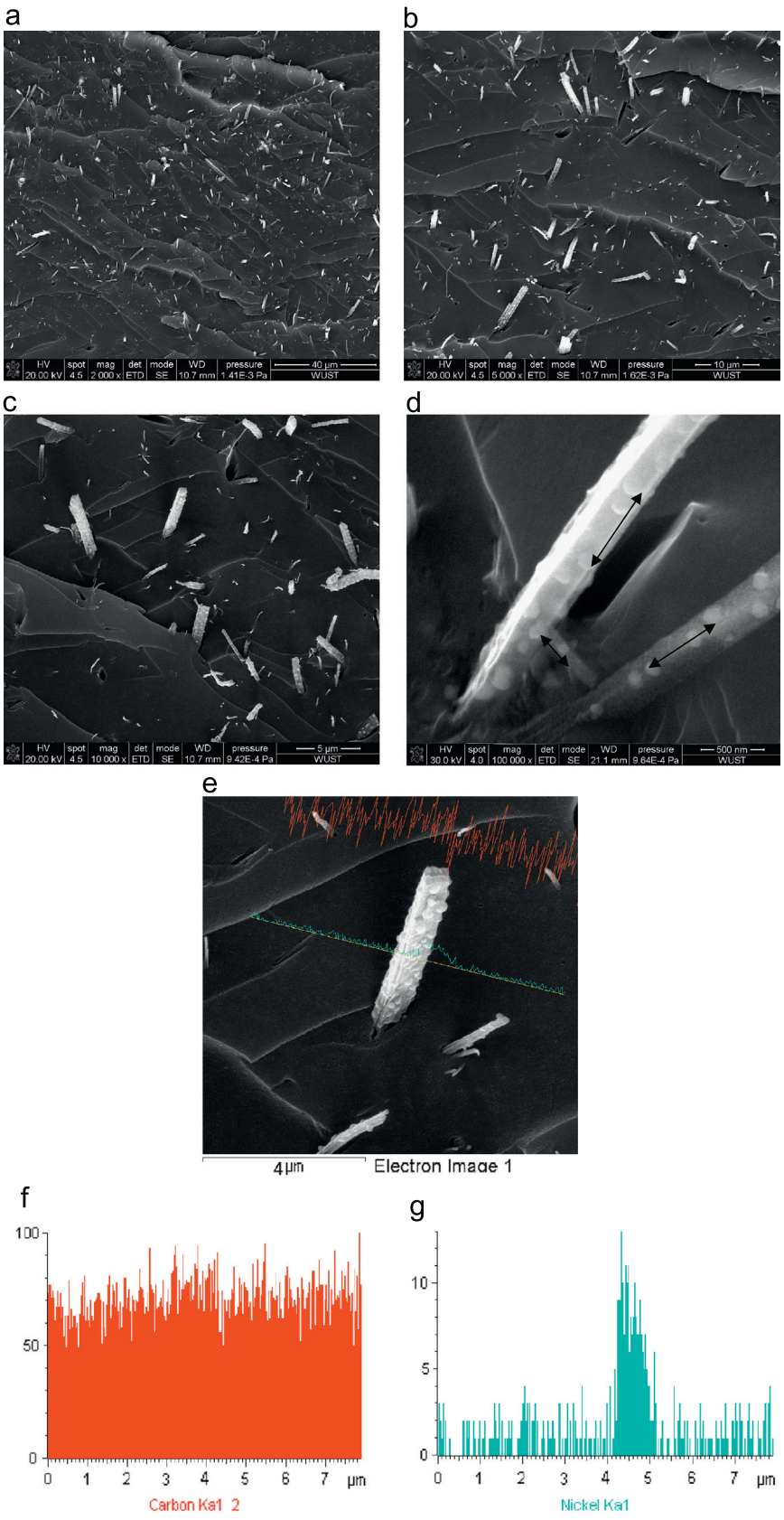

Fig. 4. SEM images of cross-section views of the $NiC_2O_4 \cdot 2H_2O$/phenolic resin composite under different magnifications treated at 1273 K for 2 h (a–d) and the line-scanning images of elements C and Ni (e–g).

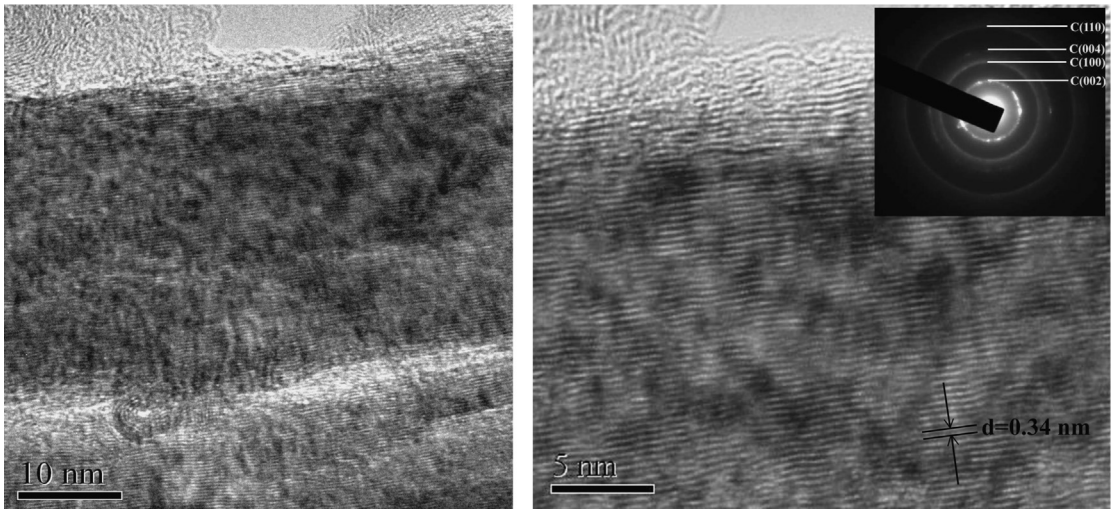

Fig. 5. TEM images (a and b) and SAED patterns (inset of b) of the graphitic carbon nanofibres obtained at 1273 K.

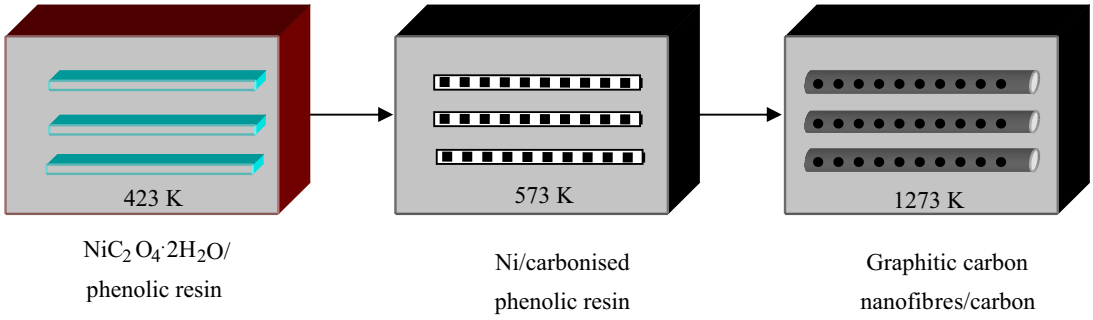

Fig. 6. Schematic diagram of the formation of graphitic carbon nanofibres.

amorphous carbon gradually decreased. This result indicated that the generated amount of graphitic carbon increases as the temperature is increased. Therefore, although the increase in temperature does not have a marked influence on the degree of structural order in the synthesised graphitic carbon, it affects the amount of graphitic structures produced.

The cross-section SEM images were used to characterise NPF treated at 1273 K for 2 h. In Fig. 4a and b, uniformly dispersed nanofibres with morphologies similar to the $NiC_2O_4 \cdot 2H_2O$ nanofibres were found on the fracture surface. Higher SEM magnification (Fig. 4c and d) revealed that the fibres on the surface of the fractures contained several dispersed nanoparticles. The EDX line-scanning image of the elemental components (Fig. 4e–g) confirms that the fibres are composed of the elements Ni and C. HRTEM and SAED were employed to further characterise the structure of the nanofibres fabricated at 1273 K. These fibres have high crystallinity (graphitic order), as evidenced by the HRTEM images (Fig. 5a and b), with well-defined C(002) lattice fringes. This result was confirmed by the SAED diffraction patterns (see inset in Fig. 5b). The d_{002} measured from the HRTEM image is 0.34 nm which is relatively close to that of graphite (0.335 nm). Thus, the C(002), C(100), C(101), and C(004) peaks in the XRD patterns in Fig. 3 are provided by the graphitic layers of carbon nanofibres.

The proposed mechanism of the formation of carbon nanofibres is shown in Fig. 6, based on the abovementioned results and analyses. Briefly, the $NiC_2O_4 \cdot 2H_2O$ nanofibres were initially uniformly trapped within the polymer matrix, surrounded by polymers, and drastically segregated from each other. At 773 K, the $NiC_2O_4 \cdot 2H_2O$ nanofibres trapped within the polymer matrix were completely decomposed and reduced into Ni nanoparticles. The presence of Ni nanoparticles helped to maintain the fibrous morphology of the $NiC_2O_4 \cdot 2H_2O$ nanofibres. As the heat treatment temperature increased, catalytic graphitisation occurred via the interaction between the Ni nanoparticles and the surrounding amorphous carbon. During this process, the metallic nanoparticles move through the neighbouring amorphous carbon while leaving behind a track of graphitic carbon nanofibres according to a dissolution–precipitation mechanism [22,23]. This result is evidenced by the SEM image in Fig. 4d, where the trajectory followed by the Ni nanoparticles is marked by an arrow. Consequently, carbon nanofibres with graphitic structures were obtained via in situ catalytic graphitisation.

During this process, the $NiC_2O_4 \cdot 2H_2O$ nanofibres act as both the catalyst precursors and templates.

4. Conclusion

We reported a novel and simple approach for preparing graphitic carbon nanofibres through the in situ catalytic graphitisation of phenolic resins using $NiC_2O_4 \cdot 2H_2O$ nanofibres as both catalyst precursors and templates. Here, graphitisation begins at 1073 K with the aid of nickel as the graphitisation catalyst. Carbon nanofibres fabricated at 1273 K have highly well-defined C(002) lattice fringes, as revealed by HRTEM. The homogeneous dispersion of $NiC_2O_4 \cdot 2H_2O$ nanofibres in the phenolic resin determined the homogeneous formation of graphitic carbon nanofibres in the matrix of the carbonised phenolic resins. The morphology, size, and concentration of the carbon nanofibres obtained in the matrix can be fine-tuned by controlling the corresponding counterparts of their catalytic precursors. The formation of graphitic carbon nanofibres was proposed to follow a dissolution–precipitation mechanism.

Acknowledgements

This work is financially supported by the National Basic Research Program of China (973 Program, No. 2012CB722702) and the Hubei Provincial Department of Education-funded Project (No. CXY2009B004).

References

[1] E. Mohoamed, M. Ewais, Carbon based refractories, Journal of the Ceramic Society 112 (2004) 517–532.
[2] X. Peng, L. Li, D. Peng, The progress of low-carbon MgO–C composite study, Refractories 37 (2003) 355–357.
[3] Z. Boquan, Z. Wenjie, Y. Yashuang, Current situation and development of low-carbon magnesia–carbon materials research, Refractories 40 (2006) 90–95.
[4] T. Ochiai, The development of refractories by applying nanotechnology, Refractories (Tokyo) 56 (2004) 152–159.
[5] V. Roungos, C.G. Aneziris, Improved thermal shock performance of Al_2O_3–C refractories due to nanoscaled additives, Ceramics International 38 (2012) 919–927.
[6] S. Tamura, T. Ochiai, T. Matsui, K.G. Giho, Technological philosophy and perspective of nano-tech refractories, Nippon Steel Technical Report 98 (2008) 18–28.
[7] S. Takanaga, T. Ochiai, S. Tamura, T. Kanai, H. Nakamura, Nanotech refractories: 2. The application of the nano structural matrix to MgO–C bricks, in: Proceedings of UNITECR'03 Congress, Osaka, Japan, 19–22 October 2003, pp. 521–524.
[8] M. Luo, Y. Li, S. Jin, S. Sang, L. Zhao, Y. Li, Microstructures and mechanical properties of Al_2O_3–C refractories with addition of multi-walled carbon nanotubes, Materials Science and Engineering: A 548 (2012) 134–141.
[9] K. Koziol, J. Vilatela, A. Moisala, M. Motta, P. Cunniff, M. Sennett, A. Windle, High-performance carbon nanotube fiber, Science 318 (2007) 1892–1895.
[10] J.N. Coleman, U. Khan, W.J. Blau, Y.K. Gun'ko, Small but strong: a review of the mechanical properties of carbon nanotube–polymer composites, Carbon 44 (2006) 1624–1652.
[11] E.T. Thostenson, Z. Ren, T. Chou, Advances in the science and technology of carbon nanotubes and their composites: a review, Composites Science and Technology 61 (2001) 1899–1912.
[12] Y. Choi, K. Sugimoto, S. Song, Y. Gotoh, Y. Ohkoshi, M. Endo, Mechanical and physical properties of epoxy composites reinforced by vapor grown carbon nanofibers, Carbon 43 (2005) 2199–2208.
[13] N. Tai, M. Yeh, J. Liu, Enhancement of the mechanical properties of carbon nanotube/phenolic composites using a carbon nanotube network as the reinforcement, Carbon 42 (2004) 2735–2777.
[14] V. Datsyuk, M. Kalyva, K. Papagelis, J. Parthenios, D. Tasis, A. Siokou, I. Kallitsis, C. Aliotis, Chemical oxidation of multiwalled carbon nanotubes, Carbon 46 (2008) 833–840.
[15] J. Yu, N. Grossiord, C.E. Koning, J. Loos, Controlling the dispersion of multi-wall carbon nanotubes in aqueous surfactant solution, Carbon 45 (2007) 618–623.
[16] X. Xie, Y. Mai, X. Zhou, Dispersion and alignment of carbonnanotubes in polymer matrix: a review, Materials Science and Engineering: R 49 (2005) 89–112.
[17] S. Kim, K. Kim, H. Ahn, K. Cho, Characterization of graphitic nanofibers synthesized by the CVD method using nickel–copper as a catalyst, Journal of Alloys and Compounds 449 (2008) 274–278.
[18] Z. Zhou, K. Liu, C. Lai, L. Zhang, J. Li, H. Hou, D.H. Reneker, H. Fong, Graphitic carbon nanofibers developed from bundles of aligned electrospun polyacrylonitrile nanofibers containing phosphoric acid, Polymer 51 (2010) 2360–2367.
[19] B. Liu, H. Yang, H. Zhao, L. An, L. Zhang, R. Shi, L. Wang, L. Bao, Y. Chen, Synthesis and enhanced gas-sensing properties of ultralong NiO nanowires assembled with NiO, Sensors and Actuators B 156 (2011) 251–262.
[20] S. Tzeng, Y. Chr, Evolution of microstructure and properties of phenolic resin-based carbon/carbon composites during pyrolysis, Materials Chemistry and Physics 73 (2002) 162–169.
[21] Z. Laušević, S. Marinković, Mechanical properties and chemistry of carbonization of phenol formaldehyde resin, Carbon 24 (1986) 575–580.
[22] O.P. Krivoruchko, V.I. Zaikovskii, A new phenomenon involving the formation of liquid mobile metal-carbon particles in the low-temperature catalytic graphitisation of amorphous carbon by metallic Fe, Co and Ni, Mendeleev communications 8 (1998) 97–99.
[23] A. Gorbunov, O. Jost, W. Pompe, A. Graff, Solid–liquid–solid growth mechanism of single-wall carbon nanotubes, Carbon 40 (2002) 113–118.